Hydrodynamics and Reactor Performance Evaluation of a High Flux Gas-Solids Circulating Fluidized Bed Downer: Experimental Study

Chengxiu Wang, Shahzad Barghi, and Jesse Zhu
Dept. of Chemical and Biochemical Engineering, The University of Western Ontario, London, Ontario, Canada N6A 5B9

DOI 10.1002/aic.14534
Published online June 30, 2014 in Wiley Online Library (wileyonlinelibrary.com)

Reactor performance of a high flux circulating fluidized bed (CFB) downer is studied under superficial gas velocities of 3–7 m/s with solids circulation rate up to 300 kg/m^{2}s using ozone decomposition reaction. Results show that the reactant conversion in the downer is closely related to the hydrodynamics, with solids holdup being the most influential parameter on ozone decomposition. High degree of conversion is achieved at the downer entrance region due to strong gas-solids interaction as well as higher solids holdup and reactant concentration. Ozone conversion increases with the increase of solids circulation rate and/or the decrease of superficial gas velocity. Overall conversion in the CFB downer is less than but very close to that in an ideal plug flow reactor indicating a good reactor performance in the downer because of the nearly "ideal" hydrodynamics in downer reactors. © 2014 American Institute of Chemical Engineers *AIChE J*, 60: 3412–3423, 2014

Keywords: high flux, circulating fluidized bed, downer, ozone decomposition, hydrodynamics, reactor performance

Introduction

Gas-solid reactors have been utilized widely in many industrial operations such as coal combustion, fluid catalytic cracking (FCC), and Fischer–Tropsch processes.[1–3] Circulating fluidized bed (CFB) is one of the efficient reactors used to handle a variety of gas-solids processes. There are two basic flow modes: the more traditional concurrent upflow in a riser and the more recently proposed concurrent downflow in a downflow CFB or downer.[4] For the riser reactor, both gas and solids are fed at the bottom and flow upward together. Compared to the conventional fluidized beds (bubbling and turbulent fluidized beds), risers have such advantages as high gas-solids contact efficiency, high solids throughput, high turn-down ration, flexible operation, and unique heat and mass transfer characteristics.[1] However, although significantly improved, the significant axial dispersion of solids which can greatly influence the selectivity and irregular distribution of the desired products, remains the main disadvantage of the CFB riser. It has been suggested that the axial back mixing in the riser is largely due to the particle aggregation which, in turn, is due to the gas and solids flow against gravity.[4]

The downer reactor, where gas and solids move downward in a concurrent fashion, has drawn much attention in recent years due to its unique features such as insignificant solids backmixing, shorter residence time, and narrow residence time distribution.[1,5] These features of downer reactors can potentially lead to its application for ultrarapid reactions such as the highly selective and fast catalytic conversion of residual oil or other hydrocarbons,[6–9] biomass, and coal pyrolysis, where narrower RTD is critical.

In chemical reactors, reactor performance is determined both by the process itself and by the hydrodynamics. The design, optimization, and scale-up of a downer reactor require more precise and quantitative understanding of both the flow behavior and the chemical reaction. Considering the numerous studies on hydrodynamics and hot model reactions in CFB riser reactors, not much efforts devoted to hydrodynamics and especially to reactor performance in downers in recent years.[2,4,9–21] Previous studies using catalytic ozone decomposition as a model reaction to evaluate reactor performance were mainly focused on gas-solids contacting in CFB risers.[22–27] To the best of our knowledge, only two research groups carried out some introductory studies on the reactor performance in downers using this model reaction. For example, Fan et al.[28,29] reported axial and radial ozone concentration profiles at very low solids circulation rate (only from 8.4 to 28.8 kg/m^{2}s) at low superficial gas velocity ranging from 2.2–3.7 m/s. However, this study did not provide the detailed kinetics, and, therefore, the experimental data may not be useful for quantitative investigation. Li et al.[3] also did some experiments using ozone decomposition reaction to study the performance of the downer reactor. They obtained comprehensive information about local solids holdup and ozone concentration profiles at different axial and radial positions at superficial gas velocities of 2–5 m/s and solids circulation rates of only 50 and 100 kg/m^{2}s. No systematic study has been conducted to investigate the hydrodynamics and reactor performance in downer reactors at high flux conditions ($G_s > 200$ kg/m^{2}s).

Correspondence concerning this article should be addressed to J. Zhu at jzhu@uwo.ca.

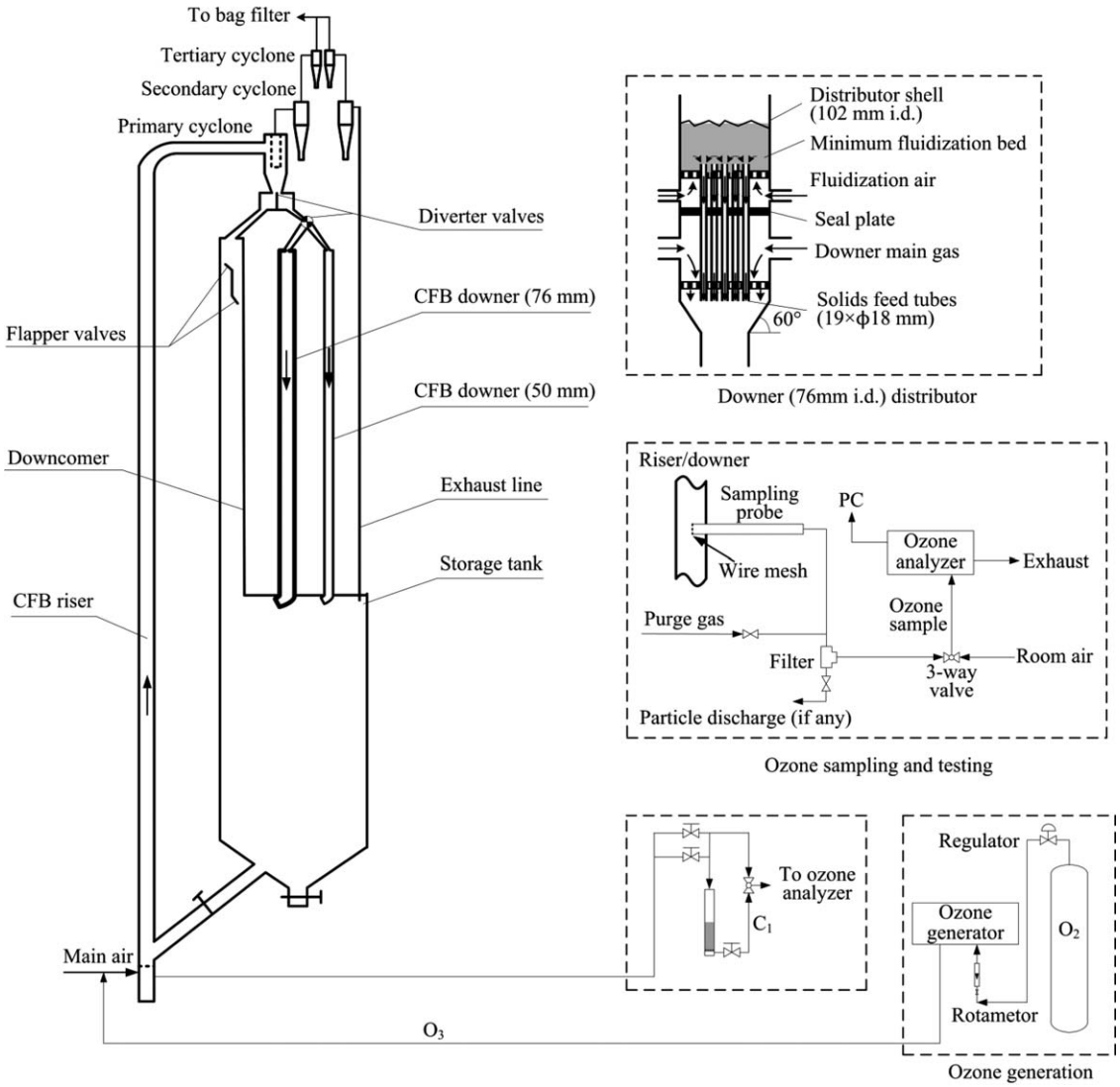

Figure 1. Schematic diagram of the multifunctional CFB and ozone testing system.

Study of chemical reactions in a downer reactor can provide direct information on its performance. To this end, the objective of this study is to obtain the axial and radial ozone concentration profiles and evaluate the downer reactor performance over a wide range of operating conditions extending to much higher solids flux well beyond those reported previously. Because of the simplicity of reaction kinetics and negligible heat effect of the reaction, the ozone decomposition reaction is chosen as a model reaction in this work. To explain the ozone profiles in the downer reactor, the hydrodynamics of the downer at the corresponding operating conditions is also determined. Finally, the reactor performances of the high flux riser and downer are compared based on two basic reactor models (completely mixed and plug flow) as well.

Experimental Details

CFB experimental system

The CFB reactor facility is shown schematically in Figure 1. The system includes three CFBs: the left hand fluidized bed serves as a high flux/density CFB riser (76 mm i.d. and 10 m high), and the right hand fluidized beds are two CFBs downer (concurrent downflow CFBs) of different diameters (76 mm i.d. and 5.8 m high and 50 mm i.d. and 4.9 m high, respectively). A large downcomer with an inner diameter of 203 mm returns solids during riser operation. At its bottom, a solids storage tank with an inner diameter up to 457 mm is used as general solids storage for the entire system. Total solids inventory of FCC particles in the downcomer and storage tank could be up to 450 kg, equivalent to a solids height of approximately 6.0 m. This high solids level ensures high back pressure in the downcomer and enables high solids circulation rates. To eliminate the effects of solids inventory and other influencing parameters on the hydrodynamic characteristics, the whole experimental work in this study is carried out with a constant particle mass of 400 kg stored in the storage tank. To obtain higher flux and steadier operating conditions, other modifications had been carried out in the CFB system reported in our previous article.[30]

When the CFB setup is under downer operating mode, solid particles are first lifted through the riser, separated by the primary cyclone fixed at the top of the downcomer and then fed into the downers. At the top of either one of the downers is a gas-solids where the particles are uniformly

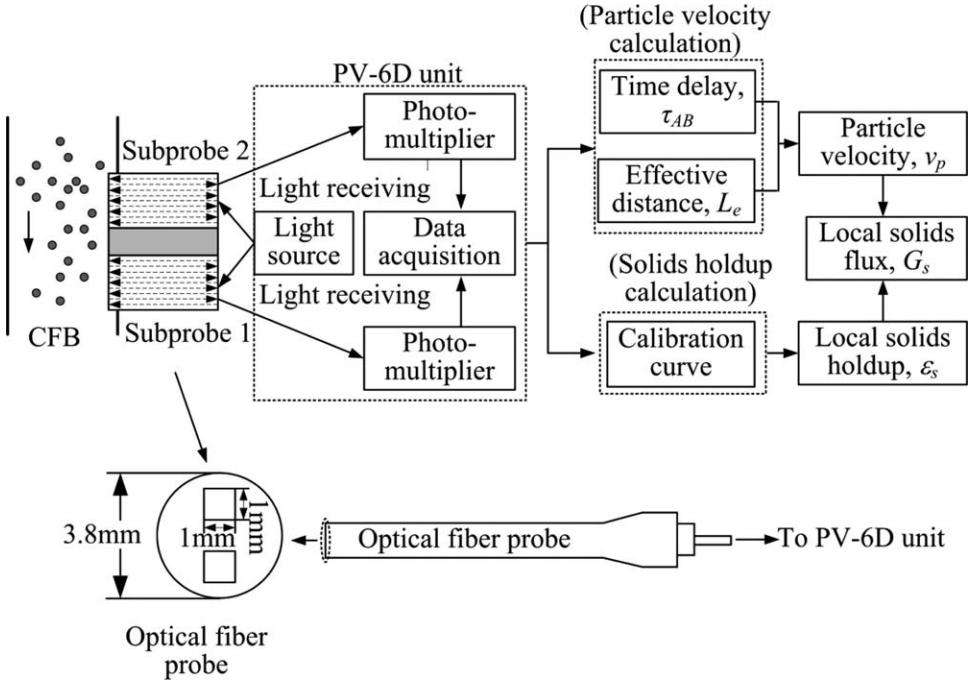

Figure 2. Schematic diagram of the new optical fiber probe and its working principle.

distributed along with the downer air to flow downward concurrently. After fast separation by gravity at the exit of either downer column, most particles are retained in the storage tank, with the remaining particles captured by two cyclones installed in series at the top of the exhausted pipeline and the common bag filter. Fine particles leaving from the baghouse return periodically to the storage tank. The gas is then discharged into the atmosphere.

The entire fluidized bed system uses aluminum as the main construction material with small portions made of Plexiglas for visual observation. To minimize possible electrostatic charges formed during the experiments, the whole fluidized bed system is electrically grounded. A measuring device for solids circulation rate is installed in the top section of the downcomer. By regulating the ball valve located in the solids feeding line connecting the storage tank and the riser column, the solids circulation rate can be adjusted and maintained at the desired level during each experiment. The solids flow rate measuring device located at the top portion of the downcomer sectioned the column into two halves with a central vertical plate and two half butterfly valves fixed at the top and the bottom of the two-half section. By appropriately flipping over the two valves from one side to the other, solids circulated through the system can be accumulated on one side of the measuring section for a given time period to provide the solids circulation rate. By regulating the ball valve located in the solids feeding line connecting the storage tank and the riser column, the solids circulation rate can be adjusted and maintained at the desired level during each experiment. Detailed measurement can be found in the previous work.[31] Main air used in this study is supplied by a large compressor capable of delivering up to 283 Nm^3/min at 241 kPa (1000 SCFM at 35 psi).

Measurement of solids holdup

Local solids holdup is measured using a newly reflective-type optical fiber probe which has been shown to be effective and accurate for measuring the local solids concentration and particle velocity in high velocity fluidized beds.[32–35] It yields high signal-to-noise ratios and is nearly free of interference by temperature, humidity, electrostatics, and electromagnetic field. Moreover, its small size does not significantly disturb the overall flow structure in CFB systems with proper design.

The optical fiber probe used in this work is model PV6D, developed by the Institute of Processing Engineering, Chinese Academy of Sciences, Beijing, China. The probe and measurement procedure are schematically shown in Figure 2. The outer diameter of the probe is 3.8 mm. The probe has two subprobes. Each of the subprobes consists of 8000 fine quartz fibers. The effective distance of the two vertically aligned subprobes is 1.51 mm, and the active tip area of each subprobe is 1×1 mm. Each subprobe consists of many quartz fibers with a diameter of 15 μm, for light-emitting and receiving, arranged in alternating arrays. To prevent particles from occupying the blind zone, a glass cover of 0.2 mm thickness is placed over the probe tip. The underlying theory is elaborated by Liu et al.[33]

As shown in Figure 2, light from the source illuminates a measuring volume of particles through the light-emitting fibers. The received light reflected by the particles is captured by light receiving fibers and processed by a photomultiplier. The light intensity is then converted into voltage signals and the voltage signals are further amplified and fed into a PC. The voltage signal obtained by the probe is converted to volumetric concentration using a calibration equation. The relationship between the output signals of the optical fiber probe and the local solids holdup (nonlinear) is first established through proper a calibration based on the method developed by Zhang et al.[36]

From the voltage time series $V(t)$ and the calibration equation, local instantaneous solids holdup, $\varepsilon_s(t)$, can be calculated

Table 1. Size Distribution of the FCC Particles

Particle Size (μm)	Volume Fraction (%)
0–20	0.61
20–40	9.72
40–60	26.32
60–80	22.80
80–130	33.24
>130	7.31

$$\varepsilon_s(t)=f[V(t)] \tag{1}$$

where, f is the calibration function. The time-mean solids concentration ε_s can be given by integrating $\varepsilon_s(t)$ over the time period, T

$$\varepsilon_s=\frac{1}{T}\int_0^T \varepsilon_s(t)dt \tag{2}$$

The cross-sectional average solids holdup $\bar{\varepsilon}_s$, can be calculated as follow

$$\bar{\varepsilon}_s=\frac{1}{\pi R^2}\int_0^R 2\pi r\varepsilon_s \mathrm{d}r=\frac{2}{R^2}\int_0^R \varepsilon_s r\mathrm{d}r \tag{3}$$

Catalyst preparation

Ozone decomposition is a thermodynamically favored process. It decomposes slowly at room temperature in the absence of catalysts, so catalysts are necessary for ozone decomposition at lower temperatures.[37–40] The noble metals such as Pt, Pd, Rh, and transition metal oxides such as MnO_2, Co_3O_4, CuO, Fe_2O_3, NiO, Ag_2O, and so forth, are the active catalysts for ozone decomposition reaction.[37] In view of the high cost of noble metals, the metal oxide catalysts are usually preferred for ozone decomposition reactions. Catalyst supports include γ-Al_2O_3, SiO_2, TiO_2, zeolite, activated carbon (or carbon fibrous materials), or a combination of these.[37,41]

The equilibrium FCC particles, impregnated with ferric nitrate are used as catalysts. FCC particles, which are primarily composed of porous amorphous aluminum hydrosilicate are activated by impregnating in a 40% (wt) solution of ferric nitrate overnight. The soaked particles are then dried and calcinated in an oven with a hood at 450°C for 4 h until no NO_2 is released. During the calcinations, the ferric nitrate is converted to ferric oxide, which is the active component for the ozone decomposition reaction. The agglomerates formed during this process are then grinded by a ball mill and sifted using a standard sieve with 250 μm pore size. The mean diameter and the particle density are 76 μm and 1780 kg/m^3 respectively. The particle-size distribution is listed in Table 1.

Ozone generation and testing

An ozone generator using the corona discharge method (Model AE15M, manufactured by Absolute Ozone) is used in this study. Using bottled oxygen as gas supply, it produces up to 30 g/h of ozone depending on the oxygen flow rate and electrical current settings. Its working pressure is 34–340 kPa (5–50 psig), with oxygen flow rate of 0.1–10 standard liter per minute. The oxygen flow rate into the generator is controlled by two rotameters (VWR, Catalog Number: 97004-648) mounted in parallel ranging from 0 to 10 LPM. The ozone/oxygen mixture exiting from the ozone generator is mixed with the main fluidization air before entering the CFB riser or downer. With a fairly long flow path and several L-bends in the main air feeding lines, the mixing process is thorough. To ensure a stable ozone supply, an output pressure of 206 kPa (30 psig) is used for the regulator installed on the oxygen gas cylinder. By simply adjusting the oxygen flow rate and electrical current settings, it is easy to obtain different amount of ozone from the ozone generator. The resulting initial ozone concentration (C_0) in the main air before ozone decomposition in the CFB downer is set to 80–100 ppm for each experiment.

An ozone analyzer (Model 49i, Thermo Electron) that uses the UV photometric method of measurement is used to measure the amount of ozone in the ozone-air sample. It is a dual-cell photometer, having both sample and reference air flowing at the same time. Each cell has a length of 37.84 cm and an inner diameter of 0.91 cm, with the internal surfaces coated with polyvinylidene fluoride to ensure that ozone undergoes no decomposition upon exposure to the internal surface of the cells (Thermo Electron, 2004 and 2005). The ozone analyzer has a measuring range of 0–200 ppm with a resolution of 0.0001 ppm ranging from 0 to 10 and 0.01 ppm for the rang of 10–200 ppm. The response time of the apparatus is 4 s. The ozone concentration output was displayed on an LCD screen. The UV source in the ozone analyzer is a 254 nm mercury lamp.

Considering the fact that ozone is highly oxidative, to reduce ozone loss in the sampling pathway to ozone analyzer, ozone-inert materials (e.g. stainless steel, copper, aluminum, and Teflon) are used for the sampling probes, valves, and piping lines (Teflon, 3 mm i.d., 6 mm o.d.). Gas samples are continuously drawn from the CFB column through a sampling system shown in Figure 1 using brass tubes (6 mm o.d. and 0.36 mm wall thickness) as the sampling probes. The tip of the probe is covered with a fine stainless steel mesh to prevent particles from being entrained into the sampling system. The velocity of gas sucked for sampling is 1.5 LPM which is low enough to assure minimal disturbance of the flow structure inside the downer. A high pressure purging air stream of 689 kPa (100 psig) is introduced to blow away any particles potentially caked in the sampling probes.

To monitor the catalyst activity during the experiments, particles were taken out from the inclined solids feeding line at the bottom of the riser. Particles of 5–10 g were used as the solids sample for catalytic activity check using the fixed bed reactor before and after each experiment. The value of the reaction rate constant (k_r) was also calculated based on the fixed bed test, which is shown in the following

$$k_r=\frac{F\rho_p}{m}\ln\left(\frac{C_0}{C_1}\right) \tag{4}$$

where k_r, apparent reaction rate constant, first order (s^{-1}), F, volumetric flow rate (m^3/s), ρ_p, particle density (kg/m^3), m, amount of catalyst particles loaded in the fixed bed reactor (g), C_0, inlet ozone concentration (ppm), C_1, outlet ozone concentration (ppm).

The value of rate constant remained 48–50 s^{-1} in this study. No significant change is observed in reaction rate constant before and after several hours of CFB run, and, therefore, the ozone concentration profiles obtained under the experimental period is assumed to be under the same particle catalytic reactivity. The average value from these two tests is taken as the reaction rate constant.

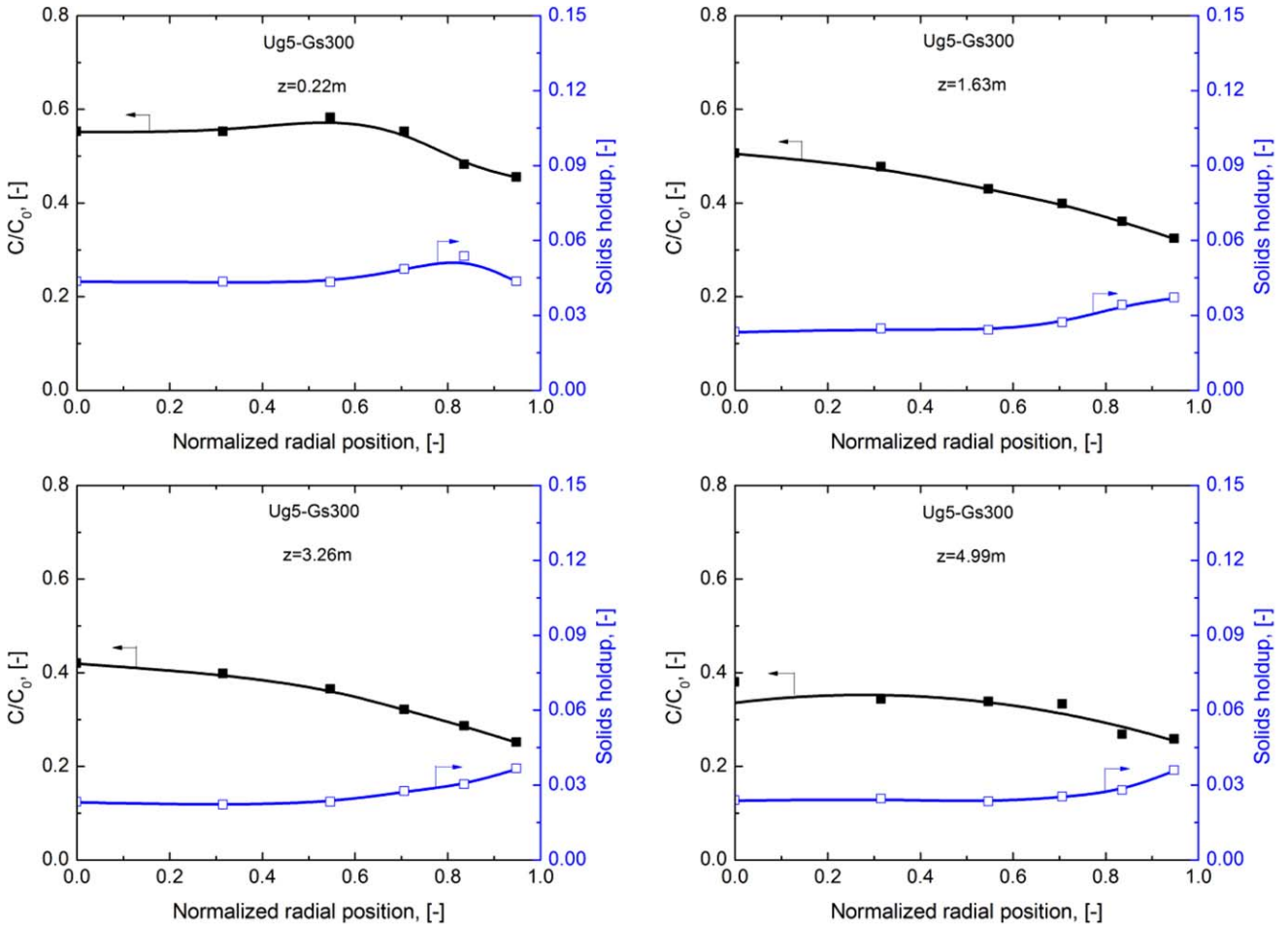

Figure 3. Radial profiles of dimensionless ozone concentration and the corresponding solids holdup.

[Color figure can be viewed in the online issue, which is available at wileyonlinelibrary.com.]

All the experiments were carried out at ambient condition in the downer with 76 mm i. d. in diameter. The temperature was monitored and recorded, however, due to the very low concentration of ozone no significant change in temperature was observed. To map the entire downer (76 mm i.d. and 5.8 m high), nine axial measuring ports ($z = 0.22$, 0.61, 1.12, 1.63, 2.13, 2.64, 3.26, 4.02, and 4.99 m below the solids distributor) are installed along the column. Measurements are conducted at six radial positions ($r/R = 0$, 0.316, 0.548, 0.707, 0.837, and 0.950, where r is the distance from the center and R is the downer radius) on each axial. These positions are determined by dividing the column cross-section into five equal areas and determining the midpoint of each of these areas. For the hydrodynamic experiments, voltage signals from the optical fiber probe are sampled at a high frequency of 100 kHz with 1,638,400 data points for each measurement. To get the valid and repeatable data, all measurements are repeated at least 5 times for each location. For the catalytic ozone decomposition, measurement is started after steady state has been reached in the CFB systems, which usually takes about at least 1 h. Ozone sampling is conducted for 1 min where the ozone concentration is fairly stable.

Results and Discussion

Radial profiles of ozone concentration

Figure 3 shows the typical radial distribution of ozone concentration and the corresponding radial solids holdup profiles along the column at the superficial gas velocity of 5 m/s and solids circulation rate of 300 kg/m^{2}s. Ozone concentrations are presented in the form of "dimensionless concentration," C/C_0, defined by ratio of the actual ozone concentration (C) measured at a certain radial position to the initial concentration (C_0) at the downer inlet. Ozone concentration is not very uniform along the radial direction. Near the entrance of the downer, the radial profile of the ozone concentration is almost flat in the central region, and decreases gradually near the wall. With increasing axial level further down the column, the radial profiles become more uniform in the central region followed by a small decrease near the wall. These radial profiles are well correlated with the radial distribution of solids holdup, plotted together in Figure 3. The radial solids flow structure is nonuniform with higher solids holdup near the wall leading to more elaborated gas-solids interactions, so that the unconverted ozone concentration is lower near the wall than that in the central region, and, therefore, the dimensionless ozone concentration near the wall is smaller than that in the central region. With the flow development along the column, the radial distributions of the solids holdup become more uniform, and so do the radial profiles of ozone concentration.

Axial profiles of ozone concentration

The cross-sectionally averaged ozone concentration profiles at different operating conditions in the downer are

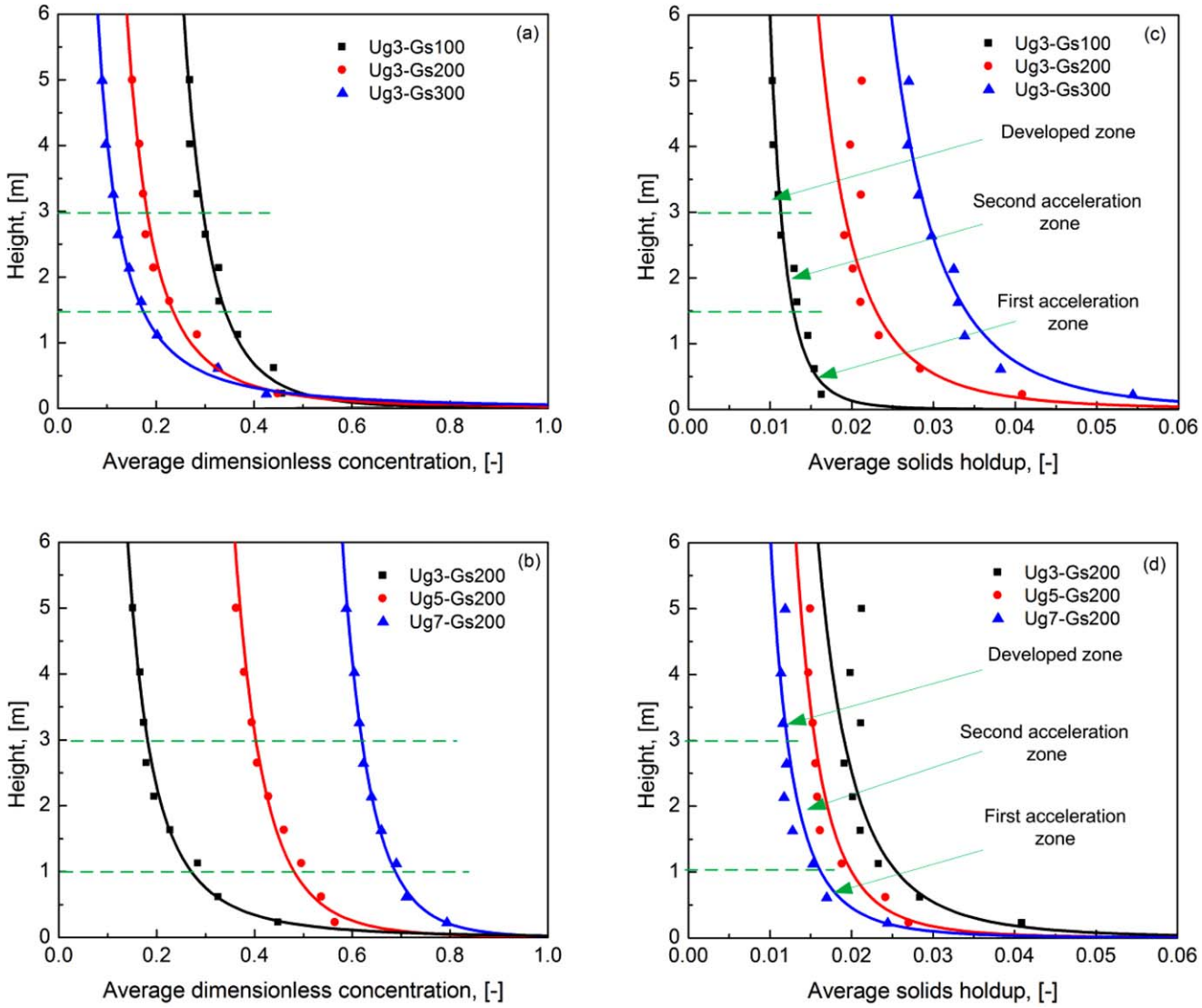

Figure 4. Axial profiles of the average dimensionless ozone concentration and the corresponding solids holdup.

[Color figure can be viewed in the online issue, which is available at wileyonlinelibrary.com.]

shown in Figure 4. The average ozone concentrations are obtained by averaging the ozone concentration at six radial positions for each axial level. In general, the dimensionless ozone concentration decreases significantly near the entrance of the column and then gradually reach a plateau further down the downer. These axial distribution profiles are consistent with those of solids holdup shown in Figures 4c, d. From Figures 4a, b, it can also be seen that larger axial gradient of ozone concentration occurs when the solids circulation rate is higher and/or when the superficial gas velocity is lower. This is reasonable since a higher solids circulation rate and/or lower gas velocity is bound to raise a higher solids holdup and contact between phases and thus higher ozone conversion.

There are three different solids flow regions along the axial direction in the downer: (1) first acceleration zone, (2) second acceleration zone, and (3) the constant velocity zone (developed zone).[1,2,12,14–16,42] In the first acceleration zone near the distributor, gas velocity is high while particle velocity is near zero. Solids are accelerated by both gravity and gas drag force until the particle velocity is equal to the gas velocity. In the second acceleration, particles are farther accelerated by gravity, but resisted by the gas drag (in the upward direction against gravity). Particle velocity then overtakes the gas velocity and increase further until gas drag on the particle counter-balances the gravity. Further downstream point, both particle and gas velocities remain constant downstream, where particles travel faster than gas, but with a constant slip velocity. Therefore, the solids holdup profiles decrease sharply in the first acceleration section near the top of the downer column, then decrease at a falling rate in the second acceleration section and finally approaches a constant value further down the downer column. The axial ozone concentration and solids holdup variations also follow this trend in axial flow structure as shown in Figure 4. Taking $U_g = 3$ m/s, $G_s = 100$ kg/m^{2}s as an example, in Figure 4c, the solids holdup decreases quickly in the top 1.5 m of the downer column, then gradually decreases up to 3 m and finally remains constant up to the downer outlet. The corresponding ozone concentration profiles shown in Figure 4a have the same trend as the solids holdup. That is to say both ozone concentration and solids holdup decrease sharply in the initial acceleration zone, then the trend becomes much smoother further down the column, and approaches a

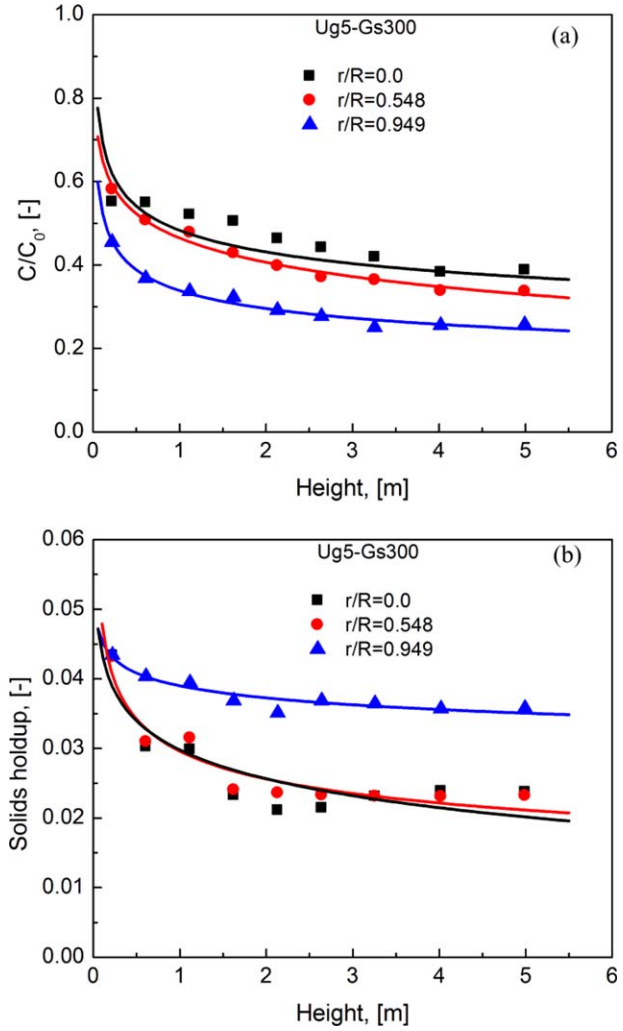

Figure 5. Axial profiles of dimensionless ozone concentration and the corresponding solids holdup at different radial positions.

[Color figure can be viewed in the online issue, which is available at wileyonlinelibrary.com.]

constant value asymptotically. Under the same G_s, the the dimensionless ozone concentration and the corresponding solids holdup have similar axial profiles as presented in Figures 4b, d.

The axial ozone concentration profiles in three radial regions and the corresponding solids holdup distributions are shown in Figure 5. Comparing the ozone changes in the three different radial positions, the ozone concentration is much lower in the wall region, given the sharply increased solids holdup. It is also seen that smaller differences between the ozone concentration profiles at $r/R = 0.0$ and $r/R = 0.548$, which correspond to the solids holdup variation against axial elevation. Moreover, ozone concentrations at the three radial positions decrease quickly along the axial direction in the first region. The variation becomes less dramatic in the second section and finally becomes nearly negligible in the third section.

Based on the above discussion, Figure 6 provides an overview of the ozone concentration and the corresponding solids holdup profiles in the downer under various operating conditions, where x and y axes are the radial and axial positions in the column, and z axis is the dimensionless ozone concentration. It is observed that with the increased distance from the solids distributor, more ozone reactants are converted due to its extended contact with the catalyst particles, giving decreased ozone concentrations. Ozone concentration in the central region is somewhat higher than that in the near wall region. The radial ozone concentration distribution also becomes uniform further down along the reactor. The impact of the operating conditions on the ozone concentration can also be seen in Figure 6. Higher U_g and/or low G_s results in relatively more uniform distribution of ozone concentration in both axial and radial directions. For example, at low solids circulation rate ($G_s = 100$ kg/m^{2}s) and high gas velocity ($U_g = 5$ m/s), the ozone concentration profiles are nearly constant along the column. More detailed information can be found in the following section.

Effect of operating conditions on ozone concentration

The effect of superficial gas velocity on ozone conversion is obviously presented in Figure 7. Generally, the concentration of the unconverted ozone increases with increasing the superficial gas velocity, under a fixed solids circulation rate of 200 kg/m^{2}s. This may be attributed to the following mechanisms: when solids circulation rate remains constant, increasing superficial gas velocity reduces the solids holdups. The decrease in solids holdup would result in the decrease of total gas-solids contacting area, which is not favorable for the reaction. Conversely, increasing superficial gas velocity leads to a short residence time of both gas and solid phases, reducing the total conversion of the reactant. Considering the above two factors, the increase of superficial gas velocity will cause the decrease of the ozone conversion. In addition, increasing U_g can lead to a more uniform radial profile of solids holdups and ozone concentrations.

The effect of solids circulation rate on radial profiles of dimensionless ozone concentration (C/C_0) at four axial levels under $U_g = 3$ m/s is shown in Figure 8. At all axial levels, the dimensionless ozone concentration decreases with an increase of solids circulation rate under the same superficial gas velocity. This is due to the solids holdups increase with increasing solids circulation rate. At high flux operating conditions, the total gas-solids contacting area for reaction and mass transfer between gas and solids will also increase leading to significant rise of the ozone conversion. Therefore, ozone concentration becomes much lower as solids circulation rate increases. Interestingly, the effect of solids circulation rate on ozone conversion seems to be much more significant in the more developed regions than that in the initial acceleration zone (near the distributor). Take one radial point, $r/R = 0$, as an example, when G_s increases from 200 to 300 kg/m^{2}s, the increment of ozone conversion is high up to 10% in the developed region ($z = 4.99$ m) while it remains unchanged near the distributor. The possible reason is that solids holdup is usually relatively high near the distributor where a change in solids circulation rate may not results in a significant change in solids holdup. Conversely, in the developed regions where particle velocity is high and solids holdup is relatively low, increasing solids circulation rate will lead to a more dramatic increase in solids holdup, given rise to better gas-solids contacting, which in turn results in high ozone conversion.

Relationship between solids holdup and ozone concentration

As aforementioned, the distribution of ozone concentration is essentially dominated by the flow structure, which can be

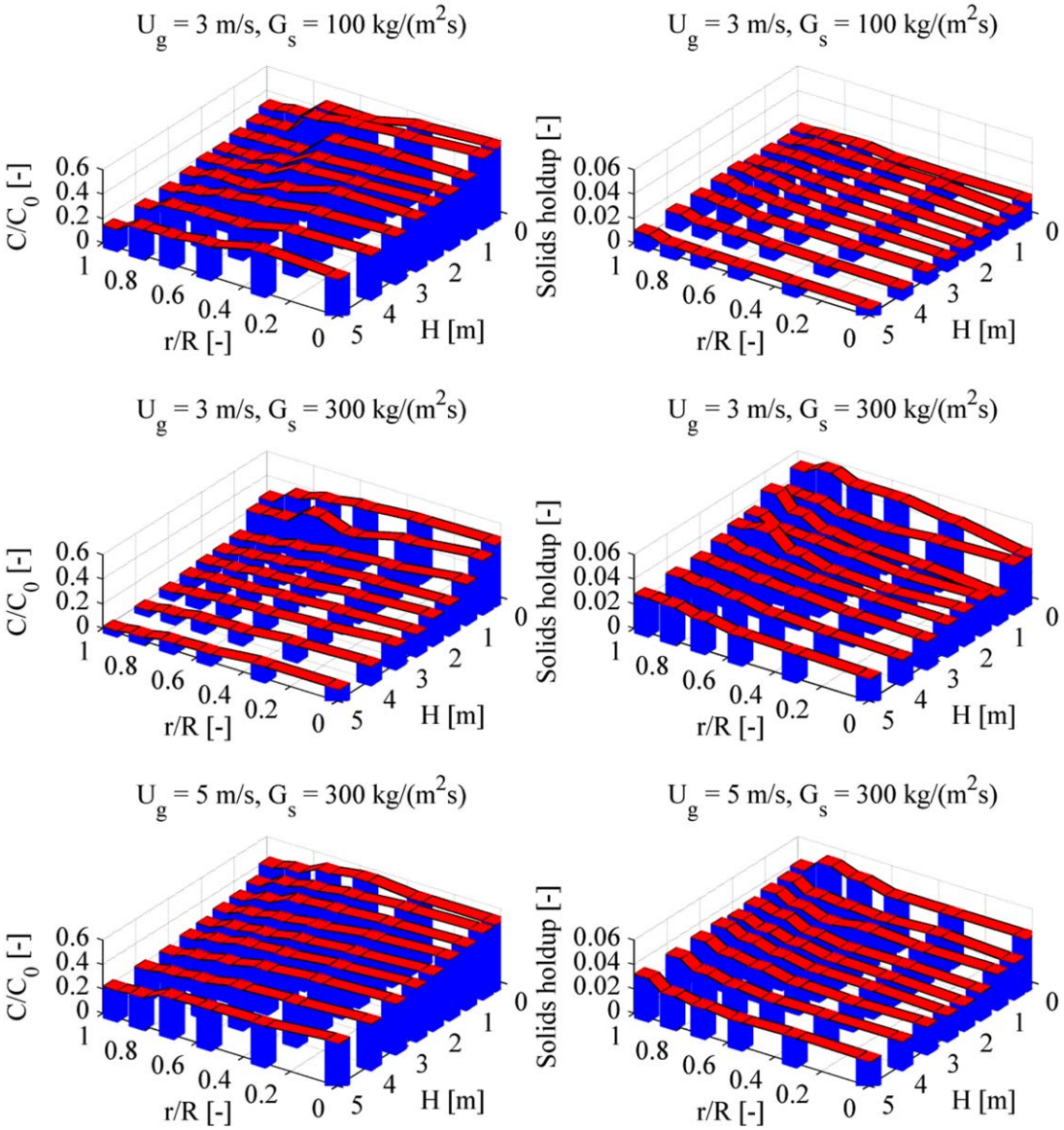

Figure 6. Overview of the dimensionless ozone concentration and the corresponding solids holdup at different operating conditions.

[Color figure can be viewed in the online issue, which is available at wileyonlinelibrary.com.]

partially represented by the solids holdup profiles in the CFB reactors. To further evaluate the effects of the solids holdup on ozone concentration, the overall conversion of ozone for the entire reactor is plotted against the mean solids holdup in the entire column as shown in Figure 9.

In general, the conversion of ozone increases with the solids holdup, as confirmed by other researchers.[3,23,26] There appears to be a linear relationship between the total ozone conversion and the mean solids holdup as shown in Figure 9. Also, the influence of solids holdup on ozone conversion is nearly the same for the three different superficial gas velocities. This phenomenon is different from that in the riser, which is also plotted in Figure 9, where the effects of solids holdup on ozone conversion are more significant under high superficial gas velocities (Wang et al.[27]), possibly due to the different hydrodynamic mechanisms in these two kinds of CFB reactors.

As shown in Figure 9, in CFB riser, higher solids holdup under higher superficial gas velocity has a much more significant effect on the overall conversion. The reason is that at low superficial gas velocities, the increase of solids holdup probably leads to the increase of cluster formation. The gas-solids mass transfer within the clusters is not as good as that between dispersed particles and the gas phase. For high superficial gas velocity conditions, the high gas velocity has more potential to break down the clusters in addition to enhancing the gas-solids contact efficiency. Therefore, the overall conversion of reactant can be increased rapidly with increasing solids holdup under high superficial gas velocity.

Conversely, the uniform distribution of solids holdup in the downer reactor is one of the key advantages over the upflow riser reactor. This is mainly because particles are not supported by the gas flow, but flow down due to the gravity, either reinforced or resisted by the drag force from the gas flow. In addition, significant aggregation of particles at the wall region can also be prevented in the downer. When particle clusters are formed, the effective drag force on the

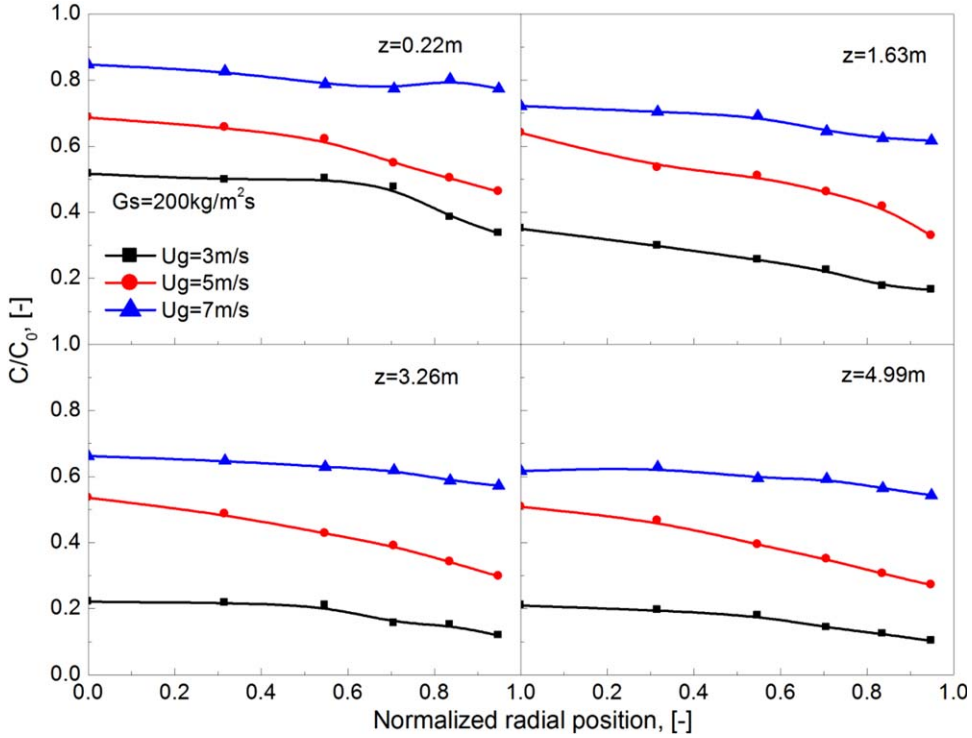

Figure 7. Effects of superficial gas velocity on the dimensionless ozone concentration.

[Color figure can be viewed in the online issue, which is available at wileyonlinelibrary.com.]

cluster is reduced so that the slip velocity becomes higher leading to a high particle downward velocity.[16] The increased particle velocity in turn increases the instability of the cluster because of the increased shear force. Large particle clusters are easily broken down into smaller ones or even isolated particles in CFB downer reactors. Therefore, the increase in solids holdup will enhance the gas-solids contacting efficiency leading to higher reactant conversion.

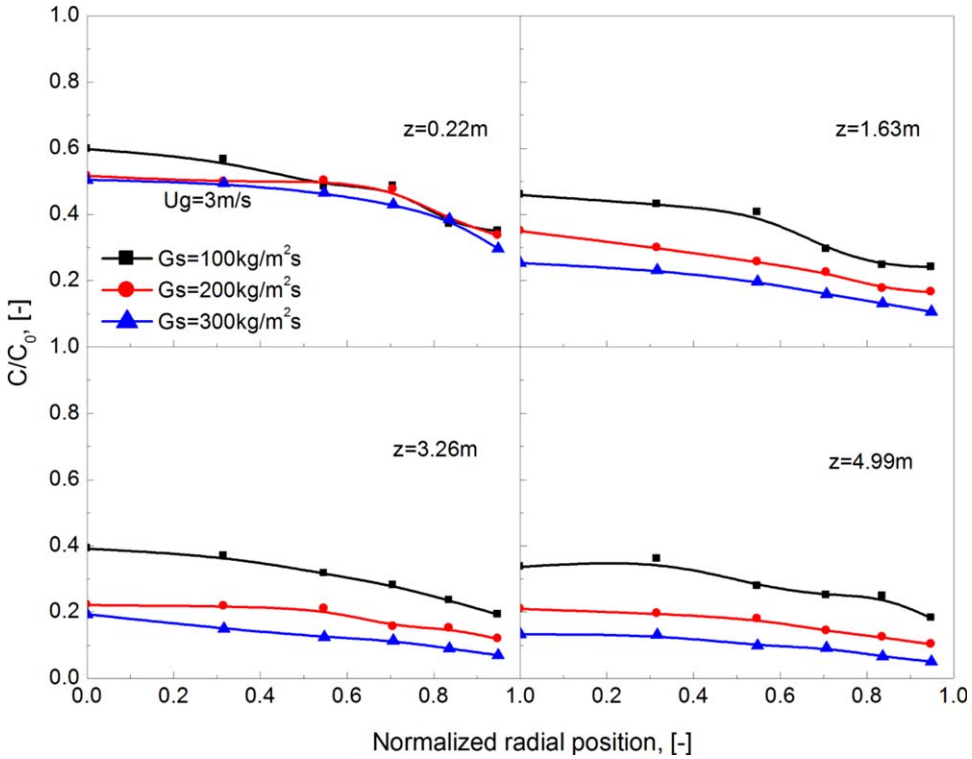

Figure 8. Effects of solids circulation rate on the dimensionless ozone concentration.

[Color figure can be viewed in the online issue, which is available at wileyonlinelibrary.com.]

Reactor performance

To gain better understanding of the CFB reactor performance, Figure 10 shows the typical results for the dependence of the overall conversion on the dimensionless kinetic rate constant (i.e., the Damköhler number $k_r' = k_r\varepsilon_s(1\text{-}\varepsilon_s)H/U_g$). As a comprehensive predictive model for the CFB reactor is not available, it is useful to choose two typical ideal reactor models: a plug flow reactor and the continuous stirred-tank reactor (CSTR) as the basis to evaluate the downer reactor performance. The conversions for PFR and CSTR have been correlated in terms of Damköhler number by Levenspiel[43]:

For PFR

$$X_{PFR} = 1 - \exp(-k_r') \tag{5}$$

For CSTR

$$X_{CSTR} = \frac{k_r'}{1 + k_r'} \tag{6}$$

The comparison of the downer reactor performance with those of the ideal model reactors is plotted in Figure 10a. Herein, it is better to note that in both Figures 10a, b, the solid line represents data in the PFR model reactor, and the dotted line represents data in the CSTR model reactor. The conversion in the CFB downer is less than (but very close to) that in the ideal PFR but significantly larger than that in the CSTR. This is expected because of the nearly "ideal" hydrodynamics in the downer reactor that very much resembles a PFR.

As the particle flow along the direction of the gravity rather than against it, the downer reactor does not display the large radial differences in both particle velocity and solids holdup.[16] When particles are no longer accelerated by the gas like that in the riser, the effect of wall friction on the gas flow (that leads to radial nonuniformity of the gas low) has little effect on the radial particles flow distribution, so that the latter becomes more uniform. Second, in the downer particles travel downward faster than the gas in the fully developed region.[1] This prevents the formation of large particle aggregates: when any aggregate in the downer grows larger, it would travel faster due to gravity, which in turn increases its tendency to breaks up. (This is contrary to the riser while large particle aggregates travels slower, making them less susceptible to breakup). Therefore, no large particle aggregation near the wall in the downer, leading to a rather uniform radial distribution of solids flow, which in turn also promotes more uniform radial gas distribution.[1] All these make the downer much closer to a PFR.

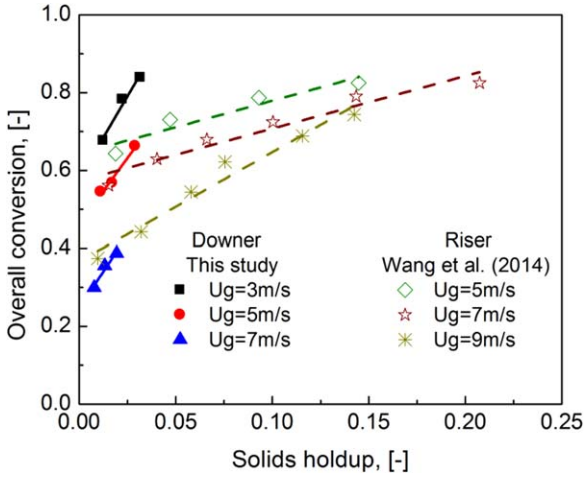

Figure 9. Relationship between overall ozone conversion and solids holdup.

[Color figure can be viewed in the online issue, which is available at wileyonlinelibrary.com.]

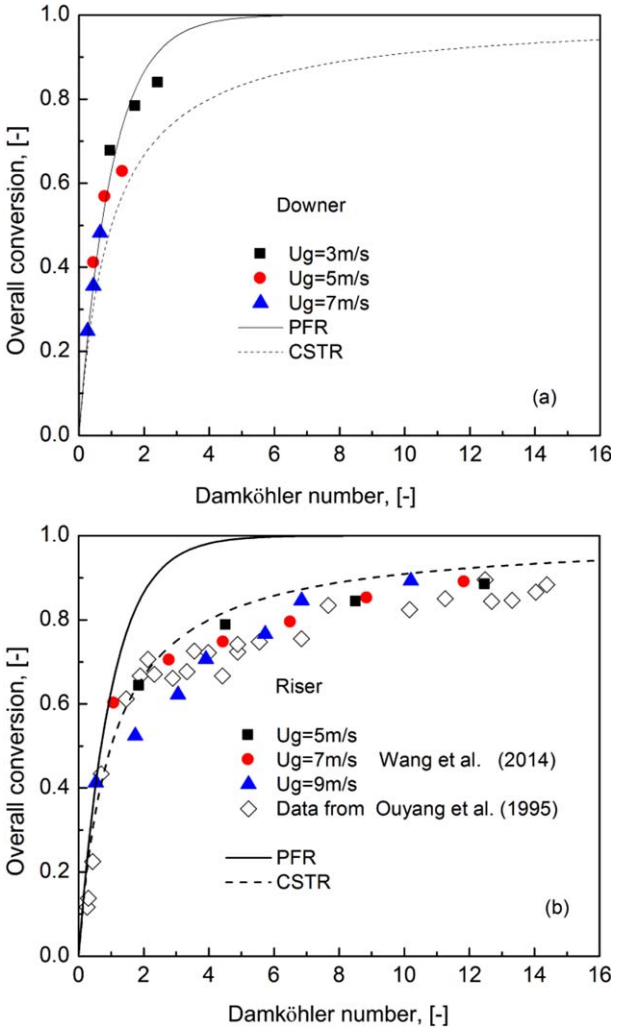

Figure 10. Reactor performance of CFB downer and riser reactors.

[Color figure can be viewed in the online issue, which is available at wileyonlinelibrary.com.]

To compare the performance in different CFB reactors, the results of the riser reported in our previous article[27] and Ouyang et al.[24,25] have also been added in Figure 10b. It is shown that the riser reactor is far from an ideal PFR reactor and in most cases performs even less than that of the CSTR except when the Damköhler number is very low. This is mainly due to the two-phase flow structure resulting from significant particle aggregations in the riser system.[6,44] Compared with the results in both riser and downer reactors, it is obvious that downer reactor performance is better than that of the riser reactor.

Conclusions

Ozone decomposition is experimentally studied in a high flux gas-solids CFB downer at superficial gas velocity of 3–

7 m/s with solids circulation rates up to 300 kg/m^{2}s, which have been carried out for the first time.

The axial and radial distribution profiles of the ozone concentration are consistent with the corresponding profiles of the solids holdups which indicate that ozone reaction in the downer is controlled by the gas-solids flow.

High ozone conversion at the entrance region of the downer indicates that the initial gas-solids contact plays a key role in the reaction yield and more attention needs to be paid on the downer distributor design, which is important to gas-solids mixing.

Ozone conversion increases with solids circulation rate under the same superficial gas velocity due to the increase of solids holdup. The conversion decreases with gas velocity at fixed solids circulation rates due to the associated reduction in solids holdup.

Overall conversion in the CFB downer is less than but very close to that in the ideal PFR indicating a good reactor performance in the downer because of the nearly "ideal" hydrodynamics in downer reactors.

Compared with the ozone conversion results in both the riser and downer reactor, it is obvious that the performance of the downer reactor is better than that of the riser reactor and will have a good prospect in both theory and application.

Notation

C_0 = initial ozone concentration, ppm
C = ozone concentration, ppm
C/C_0 = dimensionless ozone concentration, -
f = calibration function for optical fiber probe
F_s = solids flux, kg/(m^2 s)
$\bar{G}_s$ = cross-sectional average solids flux, kg/(m^2 s)
$\bar{G}_{s,L}$ = time mean local solids flux, kg/(m^2 s)
G_s = solids circulation rate, kg/(m^2 s)
k_r = reaction rate constant, s^{-1}
k_r' = Damköhler number
L_e = effective distance between light-receiving fiber 1 and 2. m
r/R = reduced radial sampling positions
t = time, s
T = time interval, s
U_g = superficial gas velocity, m/s
V = voltage, volt
$V(t)$ = voltage time series, volt
X = overall ozone conversion
z = axial coordinate, or distance from gas distributor, m

Greek letters

ε_s = solids holdup, -
$\varepsilon_s(t)$ = local instantaneous solids holdup, -
$\bar{\varepsilon}_s$ = average solids holdup in the entire column, -

Subscripts

1, 2 = subprobe 1 and 2 of optical fiber probe
g = Gas
p = Particle
s = Solids

Literature Cited

1. Zhu JX, Yu ZQ, Jin Y, Grace JR, Issangya A. Cocurrent downflow circulating fluidized bed (downer) reactors—a state of the art review. *Can J Chem Eng*. 1995;73(5):662–677.
2. Zhang H, Huang WX, Zhu JX. Gas-solids flow behavior: CFB riser vs. downer. *AIChE J*. 2001;47(9):2000–2011.
3. Li D, Zhu J, Ray MB, Ray AK. Catalytic reaction in a circulating fluidized bed downer: ozone decomposition. *Chem Eng Sci*. 2011; 66(20):4615–4623.
4. Wei F, Zhu J-X. Effect of flow direction on axial solid dispersion in gas—solids cocurrent upflow and downflow systems. *Chem Eng J Biochem Eng J*. 1996;64(3):345–352.
5. Cheng Y, Wu C, Zhu J, Wei F, Jin Y. Downer reactor: from fundamental study to industrial application. *Powder Technol*. 2008;183(3): 364–384.
6. Noymer PD, Glicksman LR. Cluster motion and particle-convective heat transfer at the wall of a circulating fluidized bed. *Int J Heat Mass Transfer*. 1998;41(1):147–158.
7. Shaikh AA, Al-Mutairi EM, Ino T. Modeling and simulation of a downer-Type HS-FCC unit. *Ind Eng Chem Res*. 2008;47(23):9018–9024.
8. Guan G, Fushimi C, Ishizuka M, Nakamura Y, Tsutsumi A, Matsuda S, Suzuki Y, Hatano H, Cheng Y, Lim C, Wang C. Flow behaviors in the downer of a large-scale triple-bed combined circulating fluidized bed system with high solids mass fluxes. *Chem Eng Sci*. 2011;66(18):4212–4220.
9. Abbasi A, Islam MA, Ege PE, de Lasa HI. CPFD flow pattern simulation in downer reactors. *AIChE J*. 2013;59(5):1635–1647.
10. Wang ZBD, Jin Y. Hydrodynamics of concurrent downflow circulating fluidized bed (CDCFB). *Powder Technol*. 1992;70:271–275.
11. Johnston PM, de Lasa HI, Zhu JX. Axial flow structure in the entrance region of downer fluidized bed: effects of the distributor design. *Chem Eng Sci*. 1999;54(13–14):2161–2173.
12. Ma Y, Zhu JX. Experimental study of heat transfer in a co-current downflow fluidized bed (downer). *Cheml Eng Sci*. 1999;54(1):41–50.
13. Schiewe T, Wirth KE, Molerus O, Tuzla K, Sharma AK, Chen JC. Measurements of solid concentration in a downward vertical gas–solid flow. *AIChE J*. 1999;45(5):949–955.
14. Zhang H, Zhu J-X, Bergougnou MA. Flow development in a gas-solids downer fluidized bed. *Can J Chem Eng*. 1999;77(2):194–198.
15. Zhang H, Zhu JX, Bergougnou MA. Hydrodynamics in downflow fluidized beds (1): solids concentration profiles and pressure gradient distributions. *Chem Eng Sci*. 1999;54(22):5461–5470.
16. Zhang H, Zhu JX. Hydrodynamics in downflow fluidized beds (2): particle velocity and solids flux profiles. *Chem Eng Sci*. 2000;55(19): 4367–4377.
17. Deng R, Liu H, Wei F, Jin Y. Axial flow structure at the varying superficial gas velocity in a downer reactor. *Chem Eng J*. 2004; 99(1):5–14.
18. Luo B, Yan D, Ma YL, Barghi S, Zhu J. Characteristics of gas–solid mass transfer in a cocurrent downflow circulating fluidized bed reactor. *Chem Eng J*. 2007;132(1–3):9–15.
19. Wu B, Zhu JX, Briens L, Zhang H. Flow dynamics in a four-inch downer using solids concentration measurements. *Powder Technol*. 2007;178(3):187–193.
20. Qi X-B, Zhang H, Zhu J. Solids concentration in the fully developed region of circulating fluidized bed downers. *Powder Technol*. 2008; 183(3):417–425.
21. Li D, Ray MB, Ray AK, Zhu J. A comparative study on hydrodynamics of circulating fluidized bed riser and downer. *Powder Technol*. 2013;247:235–259.
22. Jiang P,Jean RH, Bi H, Fan LS. Ozone decomposition in a catalytic circulating fluidized bed reactor. In: Basu MHP, Hasatani M, editors. Circulating Fluidized Bed Technology III. New York: Pergamon Press, 1990:557–562.
23. Jiang P, Bi H, Jean R-H, Fan L-S. Baffle effects on performance of catalytic circulating fluidized bed reactor. *AIChE J*. 1991;37(9): 1392–1400.
24. Ouyang S, Lin J, Potter OE. Ozone decomposition in a 0.254 m diameter circulating fluidized bed reactor. *Powder Technol*. 1993; 74(1):73–78.
25. Ouyang S, Li XG, Potter OE. Circulating fluidized bed as a catalytic reactor: experimental study. *AIChE J*. 1995;41(6):1534–1542.
26. Li D, Ray AK, Ray MB, Zhu J. Catalytic reaction in a circulating fluidized bed riser: ozone decomposition. *Powder Technol*. 2013; 242:65–73.
27. Wang C, Wang G, Li C, Barghi S, Zhu J. Catalytic ozone decomposition in a high density circulating fluidized bed riser. *Ind Eng Chem Res*. 2014;53(16):6613–6623.
28. Fan C, Zhang Y, Bi X, Song W, Lin W, Luo La. Evaluation of downer reactor performance by catalytic ozone decomposition. *Chem Eng J*. 2008;140(1–3):539–554.
29. Fan C, Bi X, Lin W, Song W. Mass transfer and reaction performance of the downer and its hydrodynamic explanation. *Can J Chem Eng*. 2008;86(3):436–447.

30. Wang C, Zhu J, Barghi S, Li C. Axial and radial development of solids holdup in a high flux/density gas–solids circulating fluidized bed. *Chem Eng Sci*. 2014;108(28):233–243.
31. Wang C. High-Density Gas-Solids Circulating Fluidized Bed Riser and Downer Reactors. London ON, Canada: Western University, 2013.
32. Johnsson H, Johnsson F. Measurements of local solids volume-fraction in fluidized bed boilers. *Powder Technol*. 2001;115(1):13–26.
33. Liu J, Grace JR, Bi X. Novel multifunctional optical-fiber probe: I. *Development and validation. AIChE J*. 2003;49(6):1405–1420.
34. Liu J, Grace JR, Bi X. Novel multifunctional optical-fiber probe: II. *High-density CFB measurements. AIChE J*. 2003;49(6):1421–1432.
35. Ellis N, Bi HT, Lim CJ, Grace JR. Influence of probe scale and analysis method on measured hydrodynamic properties of gas-fluidized beds. *Chem Eng Sci*. 2004;59(8–9):1841–1851.
36. Zhang H, Johnston PM, Zhu JX, de Lasa HI, Bergougnou MA. A novel calibration procedure for a fiber optic solids concentration probe. *Powder Technol*. 1998;100(2–3):260–272.
37. Dhandapani B, Oyama ST. Gas phase ozone decomposition catalysts. *Appl Catal B*. 1997;11(2):129–166.
38. Albert Cotton GWF, Murillo CA, Bochmann M. Advanced Inorganic Chemistry. 6th ed. New York: Wiley-Interscience, 1999.
39. Wojtowicz JA. Ozone. Kirk-Othmer Encyclopedia of Chemical Technology. New York: Wiley, 2000.
40. Lin TNJ. An AM1 study of decomposition of ozone on a Cu(110) surface. *Ozone: Sci Eng*. 2002;24(1):39–47.
41. Kirschner MJ. Ozone. Ullmann's Encyclopedia of Industrial Chemistry. New York: Wiley-VCH Verlag GmbH & Co. KGaA, 2000.
42. Yang YJYL, Yu ZQ, Wang ZW, Bai DY. The radial distribution of local particle velocity in a dilute circulating fluidized bed. In: Basu MHP, editor. Circulating Fluidized Bed Technology III. Toronto, Pergamon Press, 1991:201–206.
43. Levenspiel O. Chemical Reaction Engineering, 3rd ed. New York: Wiley, c1999; 1993.
44. Rhodes M, Mineo H, Hirama T. Particle motion at the wall of a circulating fluidized bed. *Powder Technol*. 1992;70(3):207–214.

Manuscript received Dec. 28, 2013, and revision received May 19, 2014.